ROYAL SOCIETY
OF CHEMISTRY

PAPER

Check for updates

Carboxymethylcellulose modified Fe$_3$O$_4$@SiO$_2$@GdPO$_4$:Tb^{3+},Ce^{3+} nanocomposites for combined optical and magnetic fluid hyperthermia in cancer therapy

Dhanapriya Devi Yengkhom,[a] Goutam Singh Ningombam,[a] Rameshwari Heisnam,[bc] Nanaocha Sharma,[b] Rajmuhon Singh Nongmaithem [iD][a] and Francis A. S. Chipem [iD] *[a]

A stepwise synthetic method is reported for the synthesis of multifunctional, magnetic and luminescent composites with silica-coated Fe$_3$O$_4$ as the core and Ce^{3+} sensitized Tb^{3+} doped GdPO$_4$ embedded in carboxymethylcellulose. The phase composition, infrared spectra, luminescence and magnetic properties were characterized by X-ray diffraction, FTIR, photoluminescence spectroscopy and vibrating sample magnetometry, respectively. The synthesized materials exhibit high saturation magnetization and excellent luminescence properties. The composites show intense green emission at 545 nm upon excitation at 276 nm. They attain the hyperthermia temperature (~42 °C) within the threshold alternating magnetic field (5 × 10^6 kA m^{-1} s^{-1}). The samples exhibit efficient induction heating properties which is highly desirable for magnetic hyperthermia application in cancer therapy. The materials are found to have excellent biocompatibility towards the MDA-231 breast cancer cell line and A549 lung cancer cell line with their *in vitro* cell viability showing 50% and 90%, respectively, for up to 200 µg mL^{-1} concentration, and the IC$_{50}$ values reaching 154.33 ± 18.06 µg mL^{-1} and 667.45 ± 20.03 µg mL^{-1}, respectively. The synthesized multifunctional magnetic luminescent nanocomposites provide a new insight for optical imaging and therapeutic agents for hyperthermia cancer therapy.

1. Introduction

Cancer is one of the leading causes of death throughout the world.[1] Chemotherapy along with surgery and radiotherapy is the main treatment for cancer but its limitations cause high cancer mortality as it affects both normal tissue cells and cancer cells indiscriminately.[2,3] The efficacy in cancer treatments along with chemotherapy can be enhanced by developing efficient methods.[4–6] Hyperthermia, the process of increasing the temperature up to 41–46 °C to destroy tumour-affected tissues while sparing the healthy ones, is widely studied in the field of cancer therapy.[7–9] Therefore, the combination of conventional chemotherapy with hyperthermia can lead to enhancement of the cytotoxicity and

reduction of the side effects too.[10–12] Magnetic nanoparticles have been paid great attention for improving the treatment efficiency of hyperthermia cancer therapy.[13] Magnetic hyperthermia was first reported by Gilchrist *et al.* in 1957 within the external alternating magnetic field (AMF).[14] The heat generation under an AMF in magnetic nanoparticles involves mechanisms such as hysteresis loss, Neel and Brownian relaxations, and eddy current.[15–17] Moreover, these mechanisms depend on the size of nanoparticles, magnetic anisotropy, conductivity and fluid viscosity. In hyperthermia therapy, the contribution of heat generation from eddy current is negligible. The hysteresis loss also contributes to a small amount of heat generation. However, Neel and Brownian relaxations contribute to the main heat generation for considerably small-sized nanoparticles which are single domain. While Neel relaxation is effective only on superparamagnetic nanoparticles, which is due to the rotation of magnetic moments inside each nanoparticle, Brownian relaxation is related to the movement of the particles and the viscosity of the solution and applicable to all the nanoparticles, which is due to the rotation of entire

[a] *Department of Chemistry, Manipur University, Imphal, 795003, India. E-mail: francis@manipuruniv.ac.in*

[b] *Institute of Bioresources and Sustainable Development (IBSD), Imphal-795001, India*

[c] *School of Biotechnology, Kalinga Institute of Industrial Technology, OdishaBhubaneshwar, India*

© 2024 The Author(s). Published by the Royal Society of Chemistry

RSC Appl. Interfaces, 2024, **1**, 313–322 | 313

particles under the application of a magnetic field. The Neel (τ_N) and Brownian (τ_B) relaxation times of a particle are given by the following equations:

$$\tau_N = \tau_0 e^{KV_m/k_B T} \tag{1}$$

$$\tau_B = \frac{3\eta V_H}{k_B T} \tag{2}$$

where K is the anisotropy constant, V_m is the volume of the particle, k_B is the Boltzmann constant, T is the absolute temperature, η is the viscosity, and V_H is the hydrodynamic particle volume. The pre-exponential factor τ_0 is the length of time which depends on many parameters such as temperature, gyromagnetic ratios, saturation magnetization, anisotropy constant, the height of the energy barrier, *etc.* However, τ_0 is considered to be a constant in the range of 10^{-9} to 10^{-13} s. According to Rosensweig,[18] it was suggested that Neel and Brownian relaxations occur in parallel, with a relaxation time (τ_{eff}) given by

$$\tau_{eff} = \frac{\tau_N \tau_B}{(\tau_N + \tau_B)} \tag{3}$$

The heat dissipation is dependent on both the relaxation time constants and their relative contribution with particle size. Heat generation is measured by the specific absorption rate (SAR), also called the specific loss power (SLP). A higher value of SAR leads to high efficiency of magnetic fluid hyperthermia (MFH), with the shortest duration of treatment, reducing the toxic effects of magnetic nanoparticles.[19,20] The SAR value can be calculated by using the following equation:

$$SAR = C \frac{\Delta T}{\Delta t} \frac{1}{m} \tag{4}$$

where C is the specific heat capacity of water (4.18 J g^{-1} K^{-1} mol^{-1}), m is the mass of the magnetic particle per total amount of dispersion (magnetite + water) and $\frac{\Delta T}{\Delta t}$ is the initial slope of the temperature *versus* time plot.[21] The parameters that determine the SAR are the size of particles and shape of magnetic particles, magnetization of nanoparticles, magnetic interaction of dipole, agglomeration and concentration of nanoparticles, and frequency and intensity of the AMF.[22–27] It was reported that the SAR value was found to be higher with the exchange of anisotropy and surface modification.[28] In another report, the SAR value can be affected by the frequency and intensity of the AMF. Lartigue *et al.* and Guardia *et al.* reported the increase in the SAR value of nanoparticles with the increase in magnetic field strength and frequency.[29,30] The effects of the heat generated in agglomerated nanoparticles within an ac magnetic field were also studied by Eggeman.[31] However, the suitable Hf for clinical trials to be an AMF is 5×10^9 A m^{-1} s^{-1}.[22,32]

Recently, the combination of Fe_3O_4 nanoparticles and luminescent rare earth-doped inorganic nanomaterials has been of great interest in applications such as magnetic resonance imaging, biosensors, catalysts, gene carriers, drug delivery and cancer hyperthermia.[33–37] Several reports have been studied with Fe_3O_4 nanoparticles as the core and lanthanide-doped nanomaterials as the shell.[37–39] However, it was observed that the resulting magnetic-luminescent nanomaterials exhibited weak luminescence which might be due to fluorescence quenching. Therefore, a highly water-soluble and biocompatible silica layer is coated on the surface of Fe_3O_4 nanoparticles and acted as the bridge between the Fe_3O_4 core and the lanthanide-doped rare earth shell.[38,39] Surface functionalization of the magnetic-luminescent nanomaterial is also needed to improve the chemical and physiological stability as well as bioadhesion.[37,40] Carboxymethylcellulose (CMC), one of the derivatives of cellulose, which is white, odourless, water-soluble, and biocompatible, has been used in preventing the aggregation of nanomaterials as well as for the improvement of the biocompatibility of magnetic composites.[41–43]

In this study, CMC functionalized $Fe_3O_4@SiO_2@GdPO_4$:Tb^{3+},Ce^{3+} nanocomposites were successfully prepared. In these nanocomposites, Ce^{3+} acts as a sensitizer in the enhancement of Tb^{3+} emission. The results show that the nanocomposites can be potential candidates for magnetic fluid hyperthermia and optical imaging. The induction heating properties of $Fe_3O_4@SiO_2@GdPO_4$:Tb^{3+},Ce^{3+}@CMC were studied within the threshold alternating current (AC) magnetic field. A cytotoxicity assay on the A549 lung cancer cell line and MDA 231 breast cancer cell line was also performed.

2. Experimental section

2.1. Materials

Ferrous sulphate heptahydrate ($FeSO_4 \cdot 7H_2O$, Himedia, 99.5%), polyethylene glycol 4000 (PEG 4000, Merck), ethanol, tetraethyl orthosilicate ($SiC_8H_{20}O_4$, Aldrich, 99%), ammonium hydroxide (NH_4OH, Merck), gadolinium(III) acetate hydrate ($Gd(ac)_3 \cdot xH_2O$, Sigma-Aldrich, 99.9%), terbium(III) nitrate pentahydrate ($Tb(NO_3)_3 \cdot 5H_2O$, Sigma-Aldrich, 99.9%), cerium(III) carbonate hydrate ($Ce_2(CO_3)_3 \cdot xH_2O$, Sigma-Aldrich, 99.9%), sodium phosphate dibasic (Na_2HPO_4, Sigma-Aldrich, 99%), and carboxymethylcellulose sodium salt (Central Drug House) were used. Deionised water was used as the solvent.

2.2. Preparation of Fe_3O_4 nanoparticles

Typically, 0.1 M $FeSO_4 \cdot 7H_2O$ was dissolved in 100 ml of 5% PEG solution. Then 10 mL of 10 M NH_4OH was added to the solution when black precipitates appeared immediately. After stirring continuously for 2 h, the black precipitates were kept as such for 25 h. Then the sample was removed by magnetic separation.

2.3. Preparation of $Fe_3O_4@SiO_2$ nanocomposite

$Fe_3O_4@SiO_2$ nanocomposites were synthesized according to the process modified by the Stober method. In brief, 400 mg

of Fe_3O_4 nanoparticles were homogeneously dispersed in a mixture of 90 mL of ethanol and 10 mL of deionized water and sonicated for 2 h, followed by the addition of 1 mL of tetraethyl orthosilicate (TEOS). After sonication for 2 h, 2 mL of concentrated ammonia aqueous solution was added and the mixture was sonicated for 2 h. The obtained Fe_3O_4@SiO_2 nanocomposites were separated using a magnet and washed repeatedly with deionized water and acetone to remove nonmagnetic by-products.

2.4. Preparation of Fe_3O_4@SiO_2@$GdPO_4$:Tb^{3+},Ce^{3+} nanocomposites

400 mg of Fe_3O_4@SiO_2, 0.027 g of $Ce(CO_3)_3 \cdot xH_2O$, 0.0261 g of $Tb(NO_3)_3 \cdot 5H_2O$ and 0.4364 g of $Gd(ac)_3 \cdot xH_2O$ were dissolved in 40 mL distilled water and sonicated for 2 h. 200 mg of CMC was dissolved in 20 mL of water and the solution was sonicated for 2 h. Again, the solution was stirred for 1 h and 20 mL of 0.1703 g Na_2HPO_4 was added to the solution mixture. After stirring continuously for 1 h, the solution was transferred to a stainless steel autoclave and heated for 3 h at 160 °C. Then the sample was collected by magnetic separation.

2.5. Induction heating studies

Measurements of the induction heating ability of the magnetic nanoparticles and nanocomposites were performed using EASYHEAT 8310 (Ambrell, UK). The instrument was equipped with an induction coil of 6 turns and a diameter of 7 cm. The coil was passed with a fixed applied frequency of 178 kHz. Ambient temperature was maintained by the circulation of water. 2 to 15 mg of samples suspended in 1 mL of deionized water was taken in a 1.5 mL microcentrifuge tube and this was placed at the centre of the coil without touching the walls. The sample was heated using different currents of 200 A and 300 A for 10 min. The resultant magnetic field (H) generated at different applied currents (i) was calculated using the following relation

$$H = \frac{1.257 ni}{D} \, \text{Oe} \qquad (5)$$

where n is the number of turns in the coil and D is the diameter of the turn in cm. The magnetic field intensity is then converted to kA m^{-1} s^{-1} units to compare with the clinical threshold of magnetic field intensity. The heating profile was measured in the magnetic field strengths (Hf) of 3.05×10^6 (kA m^{-1} s^{-1}) and 4.58×10^6 (kA m^{-1} s^{-1}) when 200 A and 300 A of currents were respectively passing through the coils. The temperature of the system when the sample was kept in the coil was recorded using an optical temperature sensor (Photon R & D, Canada) with an accuracy of ±0.01 °C.

2.6. Cell viability studies: MTT assay

The National Centre for Cell Science (NCCS) in Pune provided the HeLa cancer cell line and human breast cancer cell line MDA-231. The cell lines were grown in Dulbecco's modified Eagle medium (DMEM) containing 10% FBS and 0.1% pen–strep. The MTT assay was used to determine the biocompatibility and cytotoxicity of the nanocomposites at varied concentrations. After 48 hours of treatment, 15 μL MTT solution (5 mg ml^{-1}) was added to each well and incubated in an incubator for another 3 hours. During this time, formazan crystals developed and were dissolved by adding 100 L of DMSO to each well, and absorbance was measured at 570 nm using a Varioskan™ LUX multimode microplate reader.[44]

2.7. Characterization

Powder XRD was carried out on the samples using a PANalytical X-ray diffractometer (X'Pert Pro) with Cu Kα radiation (λ = 1.5405 Å) at a 2θ range of 15–70° to determine the identification and purity of the phase. The size and shape of the synthesized magnetic nanoparticles and nanocomposites were observed under a transmission electron microscope (JEOL JEM-2100, Japan). Fourier transform infrared (FTIR) spectroscopy was used to identify the functional groups present in the synthesized samples using a PerkinElmer Spectrum Two instrument. Magnetic measurements were carried out on a vibrating sample magnetometer (VSM) at room temperature using a Lakeshore VSM 7410 instrument in an applied magnetic field of ±1.5 T. The magnetization studies were performed in the powder state. Photoluminescence study of the sample was performed on a Hitachi F-7000 FL spectrophotometer with a 150 W xenon lamp as a light source. A thin film of samples was spread on a glass slide with the help of methanol and dried before taking the reading. The contents of iron and manganese in the synthesized nanocomposites were determined by inductively coupled plasma optical emission spectroscopy (ICP-OES) using a Perkin Elmer OPTIMA 5300 DV ICP-OES.
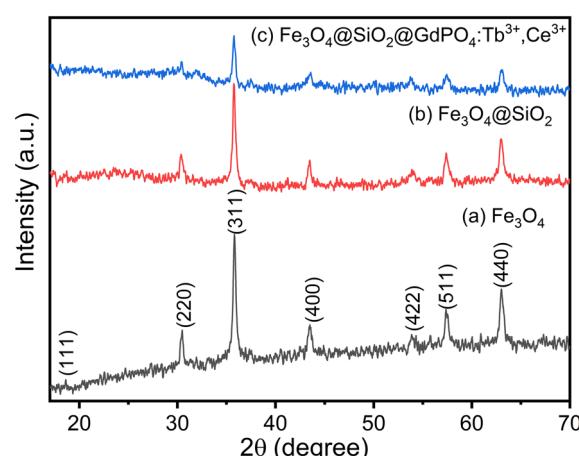
Fig. 1 XRD pattern of (a) Fe_3O_4 nanoparticles, (b) Fe_3O_4@SiO_2 nanocomposites and (c) CMC functionalized Fe_3O_4@SiO_2@$GdPO_4$:Tb^{3+},Ce^{3+} nanocomposites.

© 2024 The Author(s). Published by the Royal Society of Chemistry

RSC Appl. Interfaces, 2024, **1**, 313–322 | 315

3. Results and discussion

3.1. XRD study

The phase and crystallinity of the as-prepared samples were determined using powder X-ray diffraction (XRD) patterns. The XRD patterns of Fe_3O_4 nanoparticles with diffraction peaks at 18.61 (111), 30.52 (220), 35.83 (311), 43.53 (400), 53.88 (422), 57.37 (511) and 63.01 (440) correspond to the standard cubic structure of Fe_3O_4 with reference no. 01-075-0449 and are shown in Fig. 1(a). The estimated crystallite size of Fe_3O_4 nanoparticle is found to be 21 nm using the Scherrer equation. The estimated value is in good agreement with the TEM image as shown in Fig. 2(a). The XRD patterns of $Fe_3O_4@SiO_2$ and CMC functionalized $Fe_3O_4@SiO_2@GdPO_4:Tb^{3+},Ce^{3+}$ nanocomposites are shown in Fig. 1(b) and (c). The intensities of peaks corresponding to

Fe_3O_4 are observed to be decreased on coating with SiO_2, $GdPO_4$ and CMC. There are no peaks from SiO_2 in Fig. 1(b) which is due to the amorphous nature of the silica shell. This may be related to the formation of small-sized particles of $GdPO_4:Tb^{3+},Ce^{3+}$.[20]

3.2. TEM study

The surface morphologies of the Fe_3O_4 nanoparticles and CMC functionalized $Fe_3O_4@SiO_2@GdPO_4:Tb^{3+},Ce^{3+}$ nanocomposites are observed by the TEM images as shown in Fig. 2a and b. The Fe_3O_4 nanoparticles aggregate to have an average cluster size of ~25 nm which is shown in Fig. 2a. When the Fe_3O_4 nanoparticles are modified by CMC and coated with silica, the average size of the CMC functionalized $Fe_3O_4@SiO_2@GdPO_4:Tb^{3+},Ce^{3+}$ nanocomposite is found to be
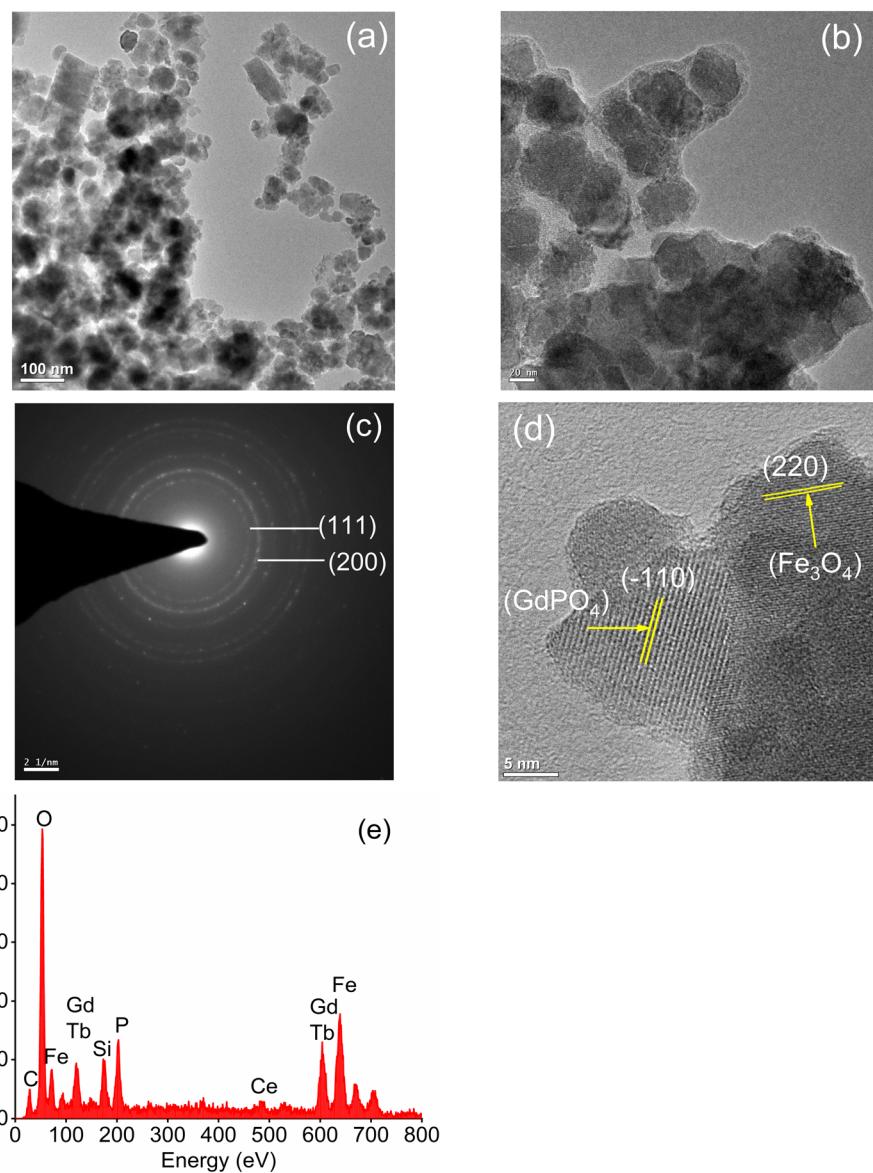
Fig. 2 TEM images of (a) Fe_3O_4 nanoparticles and (b) CMC functionalized $Fe_3O_4@SiO_2@GdPO_4:Tb^{3+},Ce^{3+}$ nanocomposites. (c) SAED pattern of Fe_3O_4 nanoparticles, (d) HRTEM image and (e) EDS spectra of CMC functionalized $Fe_3O_4@SiO_2@GdPO_4:Tb^{3+},Ce^{3+}$ nanocomposites.

© 2024 The Author(s). Published by the Royal Society of Chemistry

40–50 nm (Fig. 2b) which is bigger than that of Fe_3O_4 because of the contribution of surface SiO_2, $GdPO_4$:Tb^{3+},Ce^{3+} and CMC over core Fe_3O_4. In the picture, the formation of the core/shell type compound is clearly seen. The dotted rings of the selected area electron diffraction (SAED) patterns can be indexed very well to different diffraction planes of Fe_3O_4 as shown in Fig. 2c. The HRTEM image (Fig. 2d) also clearly reveals the lattice planes of the magnetic Fe_3O_4 particles and luminescent $GdPO_4$:Tb^{3+},Ce^{3+} from the CMC functionalized Fe_3O_4@SiO_2@$GdPO_4$:Tb^{3+},Ce^{3+} nanocomposite. The lattice plane observed has a d-spacing of 2.94 Å and 4.72 Å which matches well with the (220) plane of Fe_3O_4 and the (−110) plane of $GdPO_4$:Tb^{3+},Ce^{3+}. Thus, the Fe_3O_4 and $GdPO_4$:Tb^{3+},Ce^{3+} particles are observed together. The energy dispersive spectrum (EDS) of the CMC functionalized Fe_3O_4@SiO_2@$GdPO_4$:Tb^{3+},Ce^{3+} nanocomposite is shown in Fig. 2e. The elements Fe, Si, O, Gd, P, Tb and Ce are detected from the CMC functionalized Fe_3O_4@SiO_2@$GdPO_4$:Tb^{3+},Ce^{3+} nanocomposite.

3.3. Elemental estimation by ICP-OES

From the ICP analysis, it is found that CMC functionalized Fe_3O_4@SiO_2@$GdPO_4$:Tb^{3+},Ce^{3+} nanocomposites contained 16.03 weight percent Fe which accounts for about 22.33 weight percent Fe_3O_4 in the sample.

3.4. FTIR study

Fig. 3(a–c) show the FTIR spectra of Fe_3O_4 nanoparticles, Fe_3O_4@SiO_2 nanocomposites and CMC functionalized Fe_3O_4@SiO_2@$GdPO_4$:Tb^{3+},Ce^{3+} nanocomposites. Strong bands are observed at ~3434 and ~1640 cm^{-1} which correspond to the stretching and bending vibration of the O–H bond. The strong sharp band at 539–567 cm^{-1} is assigned to Fe–O stretching vibration. From Fig. 3(b), the peaks at 949 and 1078 cm^{-1} arise due to symmetric and asymmetric stretching of the Si–O bond. The peaks at ~448 and 619 cm^{-1} correspond to the stretching of Gd–O and P–O bonds which
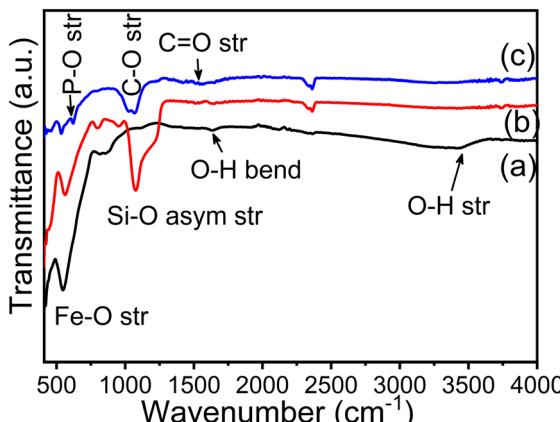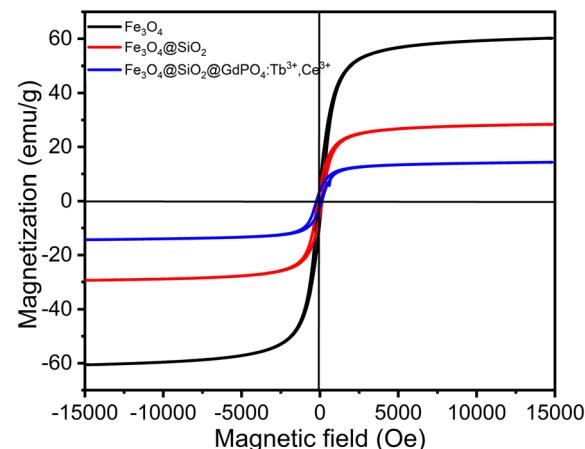

**Fig. 4** Room-temperature magnetization $vs.$ magnetic field strength for the Fe_3O_4 nanoparticle, Fe_3O_4@SiO_2 nanocomposite and CMC functionalized Fe_3O_4@SiO_2@$GdPO_4$:Tb^{3+},Ce^{3+} nanocomposite.

is observed in Fig. 3(c). The observed peaks of C–O and C=O stretching vibration at 1020–1064 cm^{-1} and 1420–1600 cm^{-1}, respectively, in Fig. 3(c) indicate that the nanoparticles are capped with CMC molecules.

3.5. Magnetization study

The magnetization (Ms) $vs.$ magnetic field (H) data for Fe_3O_4 nanoparticles, Fe_3O_4@SiO_2 nanocomposites and CMC functionalized Fe_3O_4@SiO_2@$GdPO_4$:Tb^{3+},Ce^{3+} nanocomposites are shown in Fig. 4. The respective saturation Ms values of Fe_3O_4 nanoparticles, Fe_3O_4@SiO_2 nanocomposites and CMC functionalized Fe_3O_4@SiO_2@$GdPO_4$:Tb^{3+},Ce^{3+} nanocomposites are 60.42, 28.88 and 14.32 emu g^{-1}, while the residual magnetization (Mr) values are 6.58, 3.82 and 1.93 emu g^{-1}, respectively. The low Mr value suggests that the nanoparticles are suitable for biomedical purposes. The coercivity (Hci) values of Fe_3O_4 nanoparticles, Fe_3O_4@SiO_2 nanocomposites and CMC functionalized Fe_3O_4@SiO_2@$GdPO_4$:Tb^{3+},Ce^{3+} nanocomposites are found to be 106.62 Oe, 113.58 Oe and 107.63 Oe, respectively, which suggest a slight agglomeration of particles. For application in hyperthermia, a magnetic nanocomposite with high magnetization is required. Here, the saturation magnetization (Ms) value of 14.32 emu g^{-1} would be sufficiently high enough to respond to the alternating external magnetic field during the generation of heat. Therefore, our results show that the CMC functionalized Fe_3O_4@SiO_2@$GdPO_4$:Tb^{3+},Ce^{3+} nanocomposite can be a potential candidate for hyperthermia application.

3.6. Photoluminescence study

The photoluminescence spectra of the CMC functionalized Fe_3O_4@SiO_2@$GdPO_4$:Tb^{3+},Ce^{3+} nanocomposite are shown in Fig. 5. When the emission is monitored at 545 nm, the excitation spectrum of the nanocomposite consists of two main absorption peaks at 276 nm and 307 nm, which are


Fig. 3 FTIR spectra of (a) Fe_3O_4 nanoparticles, (b) Fe_3O_4@SiO_2 nanocomposites and (c) CMC functionalized Fe_3O_4@SiO_2@$GdPO_4$:Tb^{3+},Ce^{3+} nanocomposites.

© 2024 The Author(s). Published by the Royal Society of Chemistry

RSC Appl. Interfaces, 2024, **1**, 313–322 | **317**
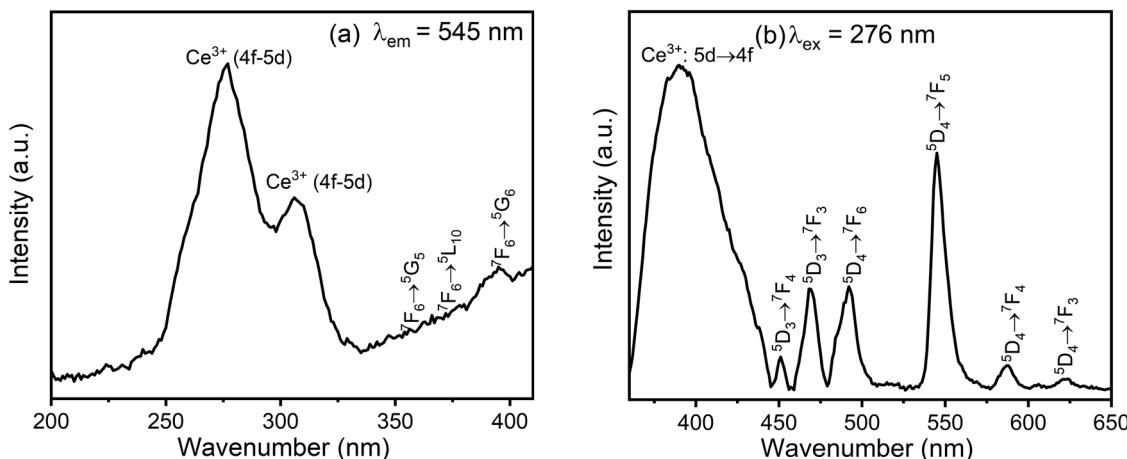
Fig. 5 (a) Excitation spectrum monitored at an emission wavelength of 545 nm and (b) emission spectrum excited at 276 nm of the CMC functionalized $Fe_3O_4@SiO_2@GdPO_4:Tb^{3+},Ce^{3+}$ nanocomposite.

associated with the spin-allowed 4f–5d transitions of Ce^{3+} from the almost degenerate electronic levels of $^2F_{5/2}$ and $^2F_{7/2}$ to the two lowest excited states of 5d orbitals, namely $^2D_{3/2}$ and $^2D_{5/2}$ (Fig. 5a). The excitation peaks observed at 356 nm, 371 nm and 395 nm are the f–f transitions $^7F_6 \rightarrow 5G_5$, $^7F_6 \rightarrow 5L_{10}$, $^7F_6 \rightarrow 5G_6$, respectively, of Tb^{3+}. The peak of the Gd^{3+} ion at ~278 nm, which is due to $^8S_{7/2} \rightarrow {}^6I_{11/2}$ transition, is merged with the spin-allowed Ce^{3+} 4f–5d transition at 276 nm so that it is not observed separately. The presence of a strong absorption peak at 276 nm as compared to f–f transition indicates the occurrence of strong energy transfer from Ce^{3+}/Gd^{3+} to the excited states of Tb^{3+}.

The emission spectrum of CMC functionalized $Fe_3O_4@SiO_2@GdPO_4:Tb^{3+},Ce^{3+}$ nanocomposite under excitation at 276 nm (Fig. 5b) shows emission bands at 450, 468, 492, 545, 588 and 623 nm attributed to the red-green emissions of $^5D_3 \rightarrow {}^7F_J$ (J = 3 and 4) and $^5D_4 \rightarrow {}^7F_J$ (J = 3, 4, 5 and 6). These peaks are assigned to the transitions of Tb^{3+}. Among these, the green emission of Tb^{3+} ion at 545 nm is the strongest because of the sensitization with Ce^{3+}.[45] The broad

emission peak in the region of 300 to 420 nm centered at 390 nm is due to the transitions from the d-level excited states of Ce^{3+} to its f-level ground state.

3.7. Induction heating studies

The induction heating profile studies of Fe_3O_4 nanoparticles and CMC functionalized $Fe_3O_4@SiO_2@GdPO_4:Tb^{3+},Ce^{3+}$ nanocomposites under different concentrations and different alternating magnetic fields of 3.05×10^6 ($kA\ m^{-1}\ s^{-1}$) and 4.58×10^6 ($kA\ m^{-1}\ s^{-1}$) are shown in Fig. 6 and 7, respectively. When the concentration of the samples and magnetic field strength increase, the temperature experienced by the samples also increases. Thus, it was observed that the heat generation increased with increase in the field strength from 3.05×10^6 to 4.58×10^6 $kA\ m^{-1}\ s^{-1}$ and the time taken to achieve the hyperthermia temperature (42 °C) becomes shorter with the increase in the concentration of magnetic nanoparticles. The respective times taken for 5, 10 and 15 mg mL^{-1} Fe_3O_4 nanoparticles are 190, 89 and 45 s at the field
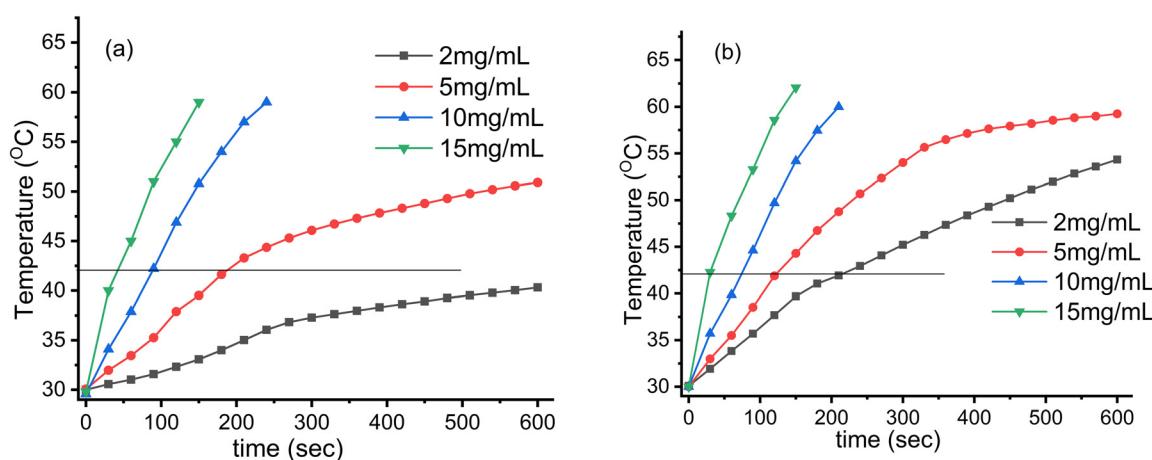

Fig. 6 Induction heating (temperature vs. time) profile of the Fe_3O_4 nanoparticles at different concentrations and magnetic field strengths (Hf) of (a) 3.05×10^6 ($kA\ m^{-1}\ s^{-1}$) and (b) 4.58×10^6 ($kA\ m^{-1}\ s^{-1}$) maintained at a fixed applied frequency of 178 kHz.
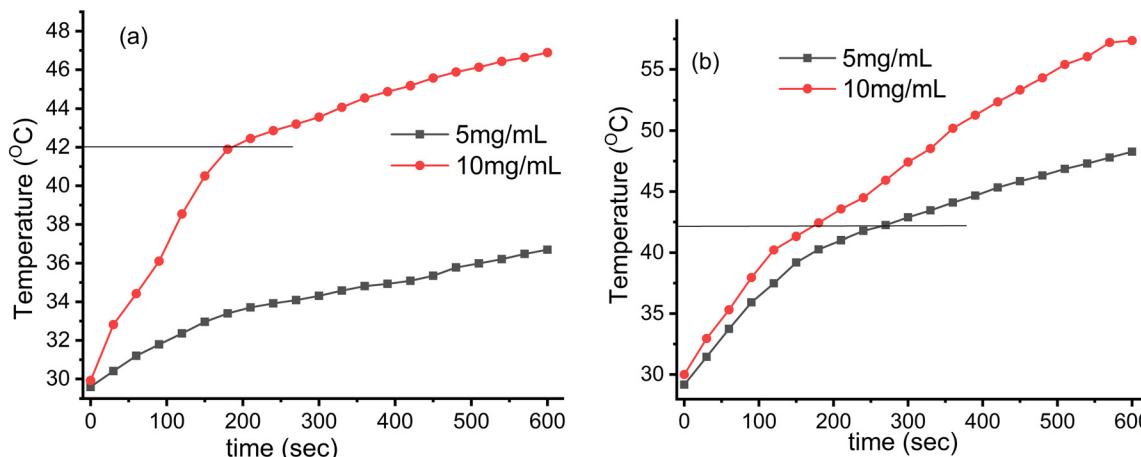
Fig. 7 Induction heating (temperature *vs.* time) profile of the $Fe_3O_4@SiO_2@GdPO_4:Tb^{3+},Ce^{3+}$ nanocomposites at different concentrations and magnetic field strengths (Hf) (a) 3.05×10^6 (kA m^{-1} s^{-1}) and (b) 4.58×10^6 (kA m^{-1} s^{-1}) maintained at a fixed applied frequency of 178 kHz.

strength of 3.05×10^6 kA m^{-1} s^{-1}, whereas the sample content of 2 mg mL^{-1} cannot attain the hyperthermia temperature (42 °C) as shown in Fig. 6a. At the field strength of 4.58×10^6 kA m^{-1} s^{-1}, all the Fe_3O_4 samples could attain the hyperthermia temperature. The times taken by the 2, 5, 10 and 15 mg mL^{-1} samples to achieve the temperature are 216, 124, 73 and 31 s, respectively, as shown in Fig. 6b.

At the field strength of 3.05×10^6 kA m^{-1} s^{-1}, the 10 mg mL^{-1} sample of CMC functionalized $Fe_3O_4@SiO_2@GdPO_4:Tb^{3+}$, Ce^{3+} nanocomposite can attain the hyperthermia temperature (42 °C) with the time taken of 186 s which is shown in Fig. 7a. With the field strength of 4.58×10^6 kA m^{-1} s^{-1}, the samples with 5 and 10 mg mL^{-1} concentrations can generate the hyperthermia temperature (42 °C) with the respective time taken being 263 and 175 s as shown in Fig. 7b.

The heat generation by magnetic nanoparticles in the alternating magnetic field is determined by SAR values. The calculated SAR values of Fe_3O_4 nanoparticles for 2, 5, 10 and 15 mg mL^{-1} samples at the field strength of 4.58×10^6 kA m^{-1} s^{-1} and 3.05×10^6 kA m^{-1} s^{-1} are respectively 130, 76, 68, 65 W g^{-1} and 46, 54, 58, 58 W g^{-1}. The calculated SAR values of the CMC functionalized $Fe_3O_4@SiO_2@GdPO_4:Tb^{3+},Ce^{3+}$ nanocomposites for 5 and 10 mg mL^{-1} samples at the field strength of 4.58×10^6 kA m^{-1} s^{-1} and 3.05×10^6 kA m^{-1} s^{-1} are respectively 57, 36 W g^{-1} and 18, 28 W g^{-1}. The heat generated by the CMC functionalized $Fe_3O_4@SiO_2@GdPO_4:Tb^{3+},Ce^{3+}$ nanocomposite is less than that generated by the Fe_3O_4 nanoparticles. This is because of the presence of non-magnetic SiO_2 coating the Fe_3O_4 in the nanocomposite, and also due to non involvement in the heat generation by $GdPO_4$ and CMC in the nanocomposite. Therefore, the SAR value of Fe_3O_4 nanoparticles is higher than that of the CMC functionalized $Fe_3O_4@SiO_2@GdPO_4:Tb^{3+},Ce^{3+}$ nanocomposites. As the present nanocomposites produce high SAR values within the acceptable range of applied magnetic fields and frequencies for hyperthermia, the studied system of nanocomposites can be potential candidates for application in clinical hyperthermia. Moreover, the SAR value was determined by not only the magnetic and morphological characteristics of

the nanoparticles but agglomeration and concentration of the nanoparticles were also taken into account for the application of nanoparticles in clinical hyperthermia. Some results indicated that the agglomeration of nanoparticles promotes an increment of the heat generated by an alternating magnetic field.[31,46] Another result also reported that the SAR value of maghemite nanoparticles was found to be enhanced when the nanoparticles are agglomerated.[47] Therefore, the agglomeration of nanoparticles is the important factor to increase the SAR value of the nanoparticles. The SAR value of the agglomerated ferrite nanoparticles was observed to be 120 W g^{-1} at an operating Hf factor of 3.12×10^6 kA m^{-1} s^{-1}.[48] In another report, the SAR values were found to be 171 W g^{-1} and 48 W g^{-1} when operated at the Hf values of 3.75×10^6 kA m^{-1} s^{-1} and 1.30×10^6 kA m^{-1} s^{-1}, respectively.[49,50] Therefore, our results suggested that the calculated SAR value of Fe_3O_4 nanoparticles might be due to the agglomerated nanoparticles and the nanoparticles could be
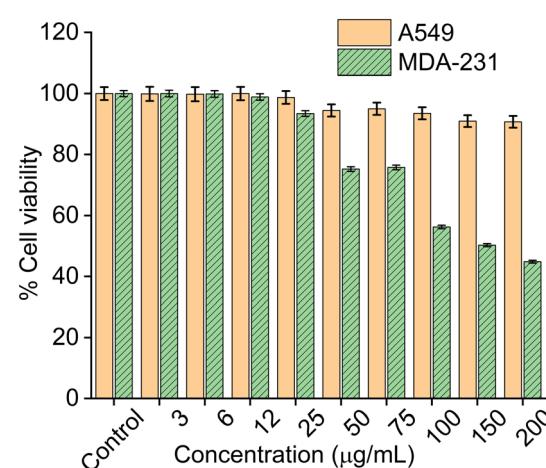

Fig. 8 *In vitro* cytotoxicity of A549 (lung cancer) cells and MDA-231 (breast cancer) cells after incubating with different concentrations of CMC functionalized $Fe_3O_4@SiO_2@GdPO_4:Tb^{3+},Ce^{3+}$ samples. The incubation period was 24 hours in all cases.

© 2024 The Author(s). Published by the Royal Society of Chemistry

RSC Appl. Interfaces, 2024, **1**, 313–322 | **319**

considered as a promising candidate as an *in vitro* hyperthermia agent in biomedicine.

3.8. Cell viability studies

Cytotoxicity studies of the CMC functionalized $Fe_3O_4@SiO_2@GdPO_4$:Tb^{3+},Ce^{3+} nanocomposite was carried out on cancer cell lines A549 and MDA-231 through MTT assay as shown in Fig. 8. Cells are incubated with CMC functionalized $Fe_3O_4@SiO_2@GdPO_4$:Tb^{3+},Ce^{3+} nanocomposite in the concentration range of 0–200 μg mL^{-1} for 48 hours. From the MTT assay result, the half maximal inhibitory concentration (IC_{50}) value of the CMC functionalized $Fe_3O_4@SiO_2@GdPO_4$:Tb^{3+},Ce^{3+} nanocomposite was calculated and found to be 667.45 ± 20.03 μg mL^{-1} for A549 and 154.33 ± 18.06 μg mL^{-1} for MDA-231. The percentage cell viability of the nanocomposite at the concentration of 200 μg mL^{-1} for A549 is 90%, whereas for MDA-231 it is 50%. The interaction of the nanocomposite with the A549 cell has no negative effect on the cell functionality thereby showing lesser toxicity. It also signifies that the nanocomposite in the A549 cells shows improved stability and biocompatibility in *in vitro* assays. Therefore, the nanocomposite is considered to be more biocompatible and less toxic to the A549 cells than to MDA-231.

4. Conclusion

The stepwise synthesis of CMC functionalized $Fe_3O_4@SiO_2@GdPO_4$:Tb^{3+},Ce^{3+} magnetic-luminescent nanocomposites was successfully performed. The nanocomposites show a strong green emission at 545 nm upon excitation at 276 nm and exhibit efficient induction heating ability under the influence of an external alternating magnetic field within the threshold Hf limit. The synthesized samples are found to show excellent biocompatibility towards the MDA-231 breast cancer cell line and A549 lung cancer cell line. *In vitro* cell viability studies have shown that the nanocomposites show 45% (MDA-231 breast cancer cell line) and 90% (A549 lung cancer cell line) viability for up to 200 μg concentrations. The IC_{50} values of the nanocomposites are found to be 154.33 ± 18.06 μg mL^{-1} and 667.45 ± 20.03 μg mL^{-1} for the MDA-231 breast cancer cell line and A549 lung cancer cell line, respectively. Therefore, these nanocomposites can serve as multimodal materials in tumor imaging and optically guided cancer hyperthermia.

Conflicts of interest

There are no conflicts to declare.

Acknowledgements

References

1 T. Sun, Y. S. Zhang, B. Pang, D. C. Hyun, M. Yang and Y. Xia, Engineered Nanoparticles for Drug Delivery in Cancer Therapy, *Angew. Chem., Int. Ed.*, 2014, **53**, 12320–12364, DOI: **10.1002/anie.201403036**.

2 R. Issels, E. Kampmann, R. Kanaar and L. H. Lindner, Hallmarks of hyperthermia in driving the future of clinical hyperthermia as targeted therapy: translation into clinical application, *Int. J. Hyperthermia*, 2016, **32**, 89–95, DOI: **10.3109/02656736.2015.1119317**.

3 T. Hehr, P. Wurst, M. Bamberg and W. Budach, Current and Potential Role of Thermoradiotherapy for Solid Tumours, *Onkologie*, 2003, **26**, 295–302, DOI: **10.1159/000071628**.

4 N. H. Levi-Polyachenko and J. H. Stewart IV, Clinical Relevance of Nanoparticle Induced Hyperthermia for Drug Delivery and Treatment of Abdominal Cancers, *Open Nanomed. J.*, 2011, **3**, 24–37, DOI: **10.2174/1875933501103010024**.

5 T. Kobayashi, Cancer hyperthermia using magnetic nanoparticles, *Biotechnol. J.*, 2011, **6**, 1342–1347, DOI: **10.1002/biot.201100045**.

6 M. Mocna, Hyperthermia in Oncology, *AIP Conf. Proc.*, 2007, **958**, 256–257, DOI: **10.1063/1.2825805**.

7 Q. Wang, Z. S. Deng and J. Liu, Theoretical evaluations of magnetic nanoparticle-enhanced heating on tumor embedded with large blood vessels during hyperthermia, *J. Nanopart. Res.*, 2012, **14**, 974, DOI: **10.1007/s11051-012-0974-6**.

8 R. Epherre, E. Duguet, S. Mornet, E. Pollert, S. Louguet, S. Lecommandoux, C. Schatz and G. Goglio, Manganite perovskite nanoparticles for self-controlled magnetic fluid hyperthermia: about the suitability of an aqueous combustion synthesis route, *J. Mater. Chem.*, 2011, **21**, 4393–4401, DOI: **10.1039/c0jm03963b**.

9 P. Wust, B. Hildebrandt, G. Sreenivasa, B. Rau, J. Gellermann, H. Riess, R. Felix and P. Schlag, Hyperthermia in combined treatment of cancer, *Lancet Oncol.*, 2002, **3**, 487–497, DOI: **10.1016/S1470-2045(02)00818-5**.

10 O. Taratula, R. K. Dani, C. Schumann, H. Xu, A. Wang, H. Song, P. Dhagat and O. Taratula, Multifunctional nanomedicine platform for concurrent delivery of chemotherapeutic drugs and mild hyperthermia to ovarian cancer cells, *Int. J. Pharm.*, 2013, **458**, 169–180, DOI: **10.1016/j.ijpharm.2013.09.032**.

11 P. Pradhan, J. Giri, F. Rieken, C. Koch, O. Mykhaylyk, M. Döblinger, R. Banerjee, D. Bahadur and C. Plank, Targeted temperature sensitive magnetic liposomes for thermo-chemotherapy, *J. Controlled Release*, 2010, **142**, 108–121, DOI: **10.1016/j.jconrel.2009.10.002**.

12 Y. Ren, H. Zhang, B. Chen, J. Cheng, X. Cai, R. Liu, G. Xia, W. Wu, S. Wang, J. Ding, C. Gao, J. Wang, W. Bao, L. Wang, L. Tian, H. Song and X. Wang, Multifunctional magnetic

320 | *RSC Appl. Interfaces*, 2024, **1**, 313–322

© 2024 The Author(s). Published by the Royal Society of Chemistry

Fe$_3$O$_4$ nanoparticles combined with chemotherapy and hyperthermia to overcome multidrug resistance, *Int. J. Nanomed.*, 2012, **7**, 2261–2269, DOI: 10.2147/IJN.S29357.

13 A. Attaluri, R. Ma, Y. Qiu, W. Li and L. Zhu, Nanoparticle distribution and temperature elevations in prostatic tumours in mice during magnetic nanoparticle hyperthermia, *Int. J. Hyperthermia*, 2011, **27**, 491–502, DOI: 10.3109/02656736.2011.584856.

14 R. K. Gilchrist, R. Medal, W. D. Shorey, R. C. Hanselman, J. C. Parrott and C. B. Taylor, Selective Inductive Heating of Lymph Nodes, *Ann. Surg.*, 1957, **146**, 596–606.

15 S. Murakami, T. Hosono, B. Jeyadevan, M. Kamitakahara and K. Ioku, Hydrothermal synthesis of magnetite/hydroxyapatite composite material for hyperthermia therapy for bone cancer, *J. Ceram. Soc. Jpn.*, 2008, **116**, 950–954, DOI: 10.2109/jcersj2.116.950.

16 A. Tampieri, T. D'Alessandro, M. Sandri, S. Sprio, E. Landi, L. Bertinetti, S. Panseri, G. Pepponi, J. Goettlicher, M. Bañobre-López and J. Rivas, Intrinsic magnetism and hyperthermia in bioactive Fe-doped hydroxyapatite, *Acta Biomater.*, 2012, **8**, 843–851, DOI: 10.1016/j.actbio.2011.09.032.

17 M. Lévy, C. Wilhelm, J. M. Siaugue, O. Horner, J. C. Bacri and F. Gazeau, Magnetically induced hyperthermia: size-dependent heating power of γ-Fe$_2$O$_3$ nanoparticles, *J. Phys.: Condens. Matter*, 2008, **20**, 204133, DOI: 10.1088/0953-8984/20/20/204133.

18 R. E. Rosensweig, Heating magnetic fluid with alternating magnetic field, *J. Magn. Magn. Mater.*, 2002, **252**, 370–374, DOI: 10.1016/S0304-8853(02)00706-0.

19 Q. Zeng, I. Baker, J. A. Loudis, Y. Liao, P. J. Hoopes and J. B. Weaver, Fe/Fe oxide nanocomposite particles with large specific absorption rate for hyperthermia, *Appl. Phys. Lett.*, 2007, **90**, 233112, DOI: 10.1063/1.2746064.

20 A. I. Prasad, A. K. Parchur, R. R. Juluri, N. Jadhav, B. N. Pandey, R. S. Ningthoujam and R. K. Vatsa, Bi-functional properties of Fe$_3$O$_4$@YPO$_4$:Eu hybrid nanoparticles: hyperthermia application, *Dalton Trans.*, 2013, **42**, 4885–4896, DOI: 10.1039/c2dt32508j.

21 C. Grüttner, K. Müller, J. Teller and F. Westphal, Synthesis and functionalisation of magnetic nanoparticles for hyperthermia applications, *Int. J. Hyperthermia*, 2013, **29**, 777–789, DOI: 10.3109/02656736.2013.835876.

22 R. Hergt and S. Dutz, Magnetic particle hyperthermia-biophysical limitations of a visionary tumour therapy, *J. Magn. Magn. Mater.*, 2007, **311**, 187–192, DOI: 10.1016/j.jmmm.2006.10.1156.

23 K. Kekalo, I. Baker, R. Meyers and J. Shyong, Magnetic Nanoparticles with High Specific Absorption Rate at Low Alternating Magnetic Field, *Nano LIFE*, 2015, **05**, 1550002, DOI: 10.1142/S1793984415500026.

24 S. Kumar, A. Daverey, V. Khalilzad-Sharghi, N. K. Sahu, S. Kidambi, S. F. Othman and D. Bahadur, Theranostics fluorescent silica encapsulated magnetic nanoassemblies for in-vitro MRI imaging and hyperthermia, *RSC Adv.*, 2015, **5**, 53180–53188, DOI: 10.1039/C5RA07632C.

25 K. R. Hurley, H. L. Ring, M. Etheridge, J. Zhang, Z. Gao, Q. Shao, N. D. Klein, V. M. Szlag, C. Chung, T. M. Reineke, M. Garwood, J. C. Bischof and C. L. Haynes, Predictable Heating and Positive MRI Contrast from a Mesoporous Silica-Coated Iron Oxide Nanoparticle, *Mol. Pharmaceutics*, 2016, **13**, 2172–2183, DOI: 10.1021/acs.molpharmaceut.5b00866.

26 M. Martínez-Carmona, M. Colilla and M. Vallet-Regí, Smart Mesoporous Nanomaterials for Antitumor Therapy, *Nanomaterials*, 2015, **5**, 1906–1937, DOI: 10.3390/nano5041906.

27 C. Haase and U. Nowak, Role of dipole-dipole interactions for hyperthermia heating of magnetic nanoparticle ensembles, *Phys. Rev. B: Condens. Matter Mater. Phys.*, 2012, **85**, 045435, DOI: 10.1103/PhysRevB.85.045435.

28 Z. Nemati, J. Alonso, L. M. Martinez, H. Khurshid, E. Garaio, J. A. Garcia, M. H. Phan and H. Srikanth, Enhanced Magnetic Hyperthermia in Iron Oxide Nano-Octopods: Size and Anisotropy Effects, *J. Phys. Chem. C*, 2016, **120**, 8370–8379, DOI: 10.1021/acs.jpcc.6b01426.

29 L. Lartigue, P. Hugounenq, D. Alloyeau, S. P. Clarke, M. Lévy, J. C. Bacri, R. Bazzi, D. F. Brougham, C. Wilhelm and F. Gazeau, Cooperative Organization in Iron Oxide Multi-Core Nanoparticles Potentiates Their Efficiency as Heating Mediators and MRI Contrast Agents, *ACS Nano*, 2012, **6**, 10935–10949, DOI: 10.1021/nn304477s.

30 P. Guardia, R. D. Corato, L. Lartigue, C. Wilhelm, A. Espinosa, M. Garcia-Hernandez, F. Gazeau, L. Manna and T. Pellegrino, Water-Soluble Iron Oxide Nanocubes with High Values of Specific Absorption Rate for Cancer Cell Hyperthermia Treatment, *ACS Nano*, 2012, **6**(4), 3080–3091, DOI: 10.1021/nn2048137.

31 A. S. Eggeman, S. A. Majetich, D. Farrell and Q. A. Pankhurst, Size and Concentration Effects on High Frequency Hysteresis of Iron Oxide Nanoparticles, *IEEE Trans. Magn.*, 2007, **43**, 2451–2453, DOI: 10.1109/TMAG.2007.894127.

32 Ö. Çelik, M. M. Can and T. Firat, Size dependent heating ability of CoFe$_2$O$_4$ nanoparticles in AC magnetic field for magnetic nanofluid hyperthermia, *J. Nanopart. Res.*, 2014, **16**, 2321, DOI: 10.1007/s11051-014-2321-6.

33 S. A. Corr, Y. P. Rakovich and Y. K. Gun'Ko, Multifunctional Magnetic-fluorescent Nanocomposites for Biomedical Applications, *Nanoscale Res. Lett.*, 2008, **3**, 87–104, DOI: 10.1007/s11671-008-9122-8.

34 J. Kim, Y. Piao and T. Hyeon, Multifunctional nanostructured materials for multimodal imaging, and simultaneous imaging and therapy, *Chem. Soc. Rev.*, 2009, **38**, 372–390, DOI: 10.1039/b709883a.

35 X. Zhu, J. Zhou, M. Chen, M. Shi, W. Feng and F. Li, Coreshell Fe$_3$O$_4$@NaLuF$_4$:Yb,Er/Tm nanostructure for MRI, CT and upconversion luminescence tri-modality imaging, *Biomaterials*, 2012, **33**, 4618–4627, DOI: 10.1016/j.biomaterials.2012.03.007.

36 S. Gai, P. Yang, C. Li, W. Wang, Y. Dai, N. Niu and J. Lin, Synthesis of Magnetic, Up-Conversion Luminescent, and

© 2024 The Author(s). Published by the Royal Society of Chemistry

RSC Appl. Interfaces, 2024, **1**, 313–322 | **321**

Mesoporous Core–Shell-Structured Nanocomposites as Drug Carriers, *Adv. Funct. Mater.*, 2010, **20**, 1166–1172, DOI: **10.1002/adfm.200902274**.

37 G. S. Ningombam, D. Chattopadhyay, K. Sarkar, S. N. Kalkura and N. R. Singh, Luminescent water dispersible core-shell – $(Y/Eu/Li)VO_4$@APTES@Folate and $(Y/Eu/Li)VO_4$@Fe_3O_4@PEG nanocomposites: Biocompatibility and induction heating within the threshold alternating magnetic field, *Colloids Surf., A*, 2021, **625**, 126826, DOI: **10.1016/j.colsurfa.2021.126826**.

38 J. Ladol, H. Khajuria, H. N. Sheikh and Y. Khajuria, Synthesis and characterization of bi-functional magneto-luminescent Fe_3O_4@SiO_2@$NaLuF_4$:Eu^{3+} hybrid core/shell nanospheres, *J. Chem. Sci.*, 2016, **128**, 1149–1155, DOI: **10.1007/s12039-016-1108-y**.

39 M. Runowski, T. Grzyb and S. Lis, Magnetic and luminescent hybrid nanomaterial based on Fe_3O_4 nanocrystals and $GdPO_4$:Eu^{3+} nanoneedle, *J. Nanopart. Res.*, 2012, **14**, 1188, DOI: **10.1007/s11051-012-1188-7**.

40 G. S. Ningombam, B. Srinivasan, A. H. Chidananda, S. N. Kalkura, Y. Sharma and N. R. Singh, Polymer modified magnetic-luminescent nanocomposites for combined optical imaging and magnetic fluid hyperthermia in cancer therapy: analysis of Mn^{2+} doping for enhanced heating effect, hemocompatibility and biocompatibility, *Dalton Trans.*, 2022, **51**, 8510–8524, DOI: **10.1039/d2dt00308b**.

41 N. Dehghani, M. Babamoradi, Z. Hajizadeh and A. Maleki, Improvement of Magnetic Property of CMC/Fe_3O_4 Nanocomposite by Applying External Magnetic Field During Synthesis, *Chem. Methodol.*, 2020, **4**, 92–99, DOI: **10.33945/SAMI/CHEMM.2020.1.8**.

42 S. A. Pour, H. R. Shaterian, M. Afradi and A. Yazdani-Elah-Abadi, Carboxymethyl Cellulose (CMC)-loaded Co-Cu Doped Manganese Ferrite Nanorods as a New Dual-Modal Simultaneous Contrast Agent for Magnetic Resonance Imaging and Nanocarrier for Drug Delivery System, *J. Magn. Magn. Mater.*, 2017, **438**, 85–94, DOI: **10.1016/j.jmmm.2017.04.069**.

43 A. Nasiri, M. Malakootian, M. A. Shiri, G. Yazdanpanah and M. Nozari, CoFe2O4@methylcellulose synthesized as a new magnetic nanocomposite to tetracycline adsorption: modeling, analysis, and optimization by response surface methodology, *J. Polym. Res.*, 2021, **28**, 192, DOI: **10.1007/s10965-021-02540-y**.

44 T. Mosmann, Rapid Colorimetric Assay for Cellular Growth and Survival: Application to Proliferation and Cytotoxicity Assays, *J. Immunol. Methods*, 1983, **65**, 55–63, DOI: **10.1016/0022-1759(83)90303-4**.

45 N. K. Sahu, N. S. Singh, L. Pradhan and D. Bahadur, Ce^{3+} sensitized $GdPO_4$:Tb^{3+} with iron oxide nanoparticles: a potential biphasic system for cancer theranostics, *Dalton Trans.*, 2014, **43**, 11728–11738, DOI: **10.1039/c4dt00792a**.

46 M. Jeun, S. Bae, A. Tomitaka, Y. Takemura, K. H. Park, S. H. Paek and K. W. Chung, Effects of particle dipole interaction on the ac magnetically induced heating characteristics of ferrite nanoparticles for hyperthermia, *Appl. Phys. Lett.*, 2009, **95**, 130–133, DOI: **10.1063/1.3211120**.

47 A. Urtizberea, E. Natividad, A. Arizaga, M. Castro and A. Mediano, Specific Absorption Rates and Magnetic Properties of Ferrofluids with Interaction Effects at Low Concentrations, *J. Phys. Chem. C*, 2010, **114**, 4916–4922, DOI: **10.1021/jp912076f**.

48 G. Goya, E. Lima Jr., A. Arelaro, T. Torres, H. Rechenberg, L. Rossi, C. Marquina and M. Ibarra, Magnetic Hyperthermia with Fe3O4 Nanoparticles: The Influence of Particle Size on Energy Absorption, *IEEE Trans. Magn.*, 2008, **44**, 4444–4447, DOI: **10.1109/TMAG.2008.2003508**.

49 M. Timko, A. Dzarova, J. Kovac, A. Skumiel, A. Józefczak, T. Hornowski, H. Gojżewski, V. Zavisova, M. Koneracka, A. Sprincova, O. Strbak, P. Kopcansky and N. Tomasovicova, Magnetic properties and heating effect in bacterial magnetic nanoparticles, *J. Magn. Magn. Mater.*, 2009, **321**, 1521–1524, DOI: **10.1016/j.jmmm.2009.02.077**.

50 E. Lima, E. De Biasi, M. V. Mansilla, M. E. Saleta, M. Granada, H. E. Troiani, F. B. Effenberger, L. M. Rossi, H. R. Rechenberg and R. D. Zysler, Heat generation in agglomerated ferrite nanoparticles in an alternating magnetic field, *J. Phys. D: Appl. Phys.*, 2013, **46**, 045002, DOI: **10.1088/0022-3727/46/4/045002**.